iScience, Volume *23*

Supplemental Information

Mitochondrial Protrusions in Neuronal Cells

Pamela J. Yao, Erden Eren, Ronald S. Petralia, Jeffrey W. Gu, Ya-Xian Wang, and Dimitrios Kapogiannis

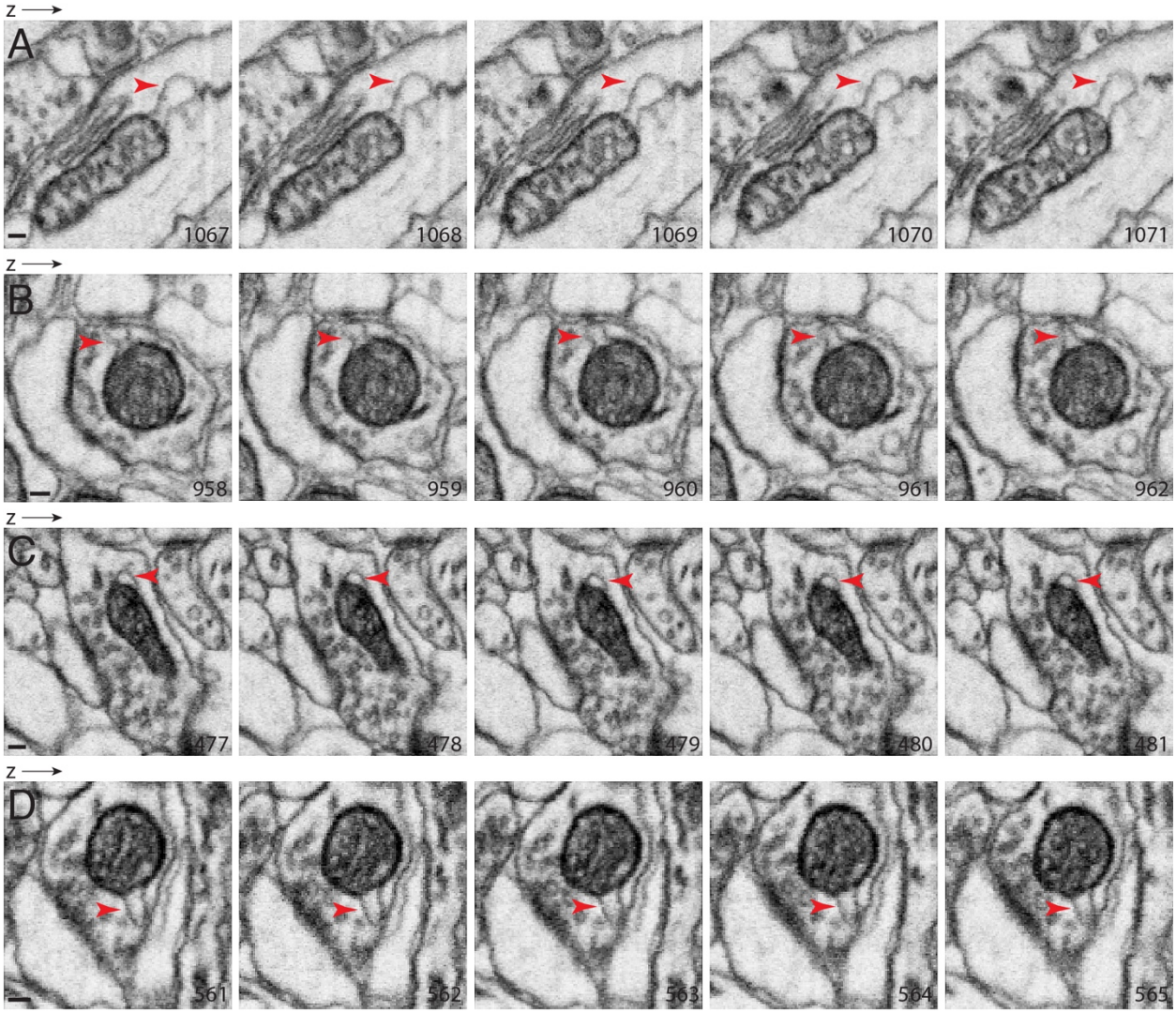

Figure S1. FIB-SEM examination of neurons in the mouse hippocampus (CA1), Related to Figure 3 & 4. (A-D) Examples of mitochondrial protrusions (arrowheads). The voxel of the FIB-SEM is 8x8x8 nm. The number on the micrograph indicates its z-position in the SEM image stack. Scale bars, 100 nm.

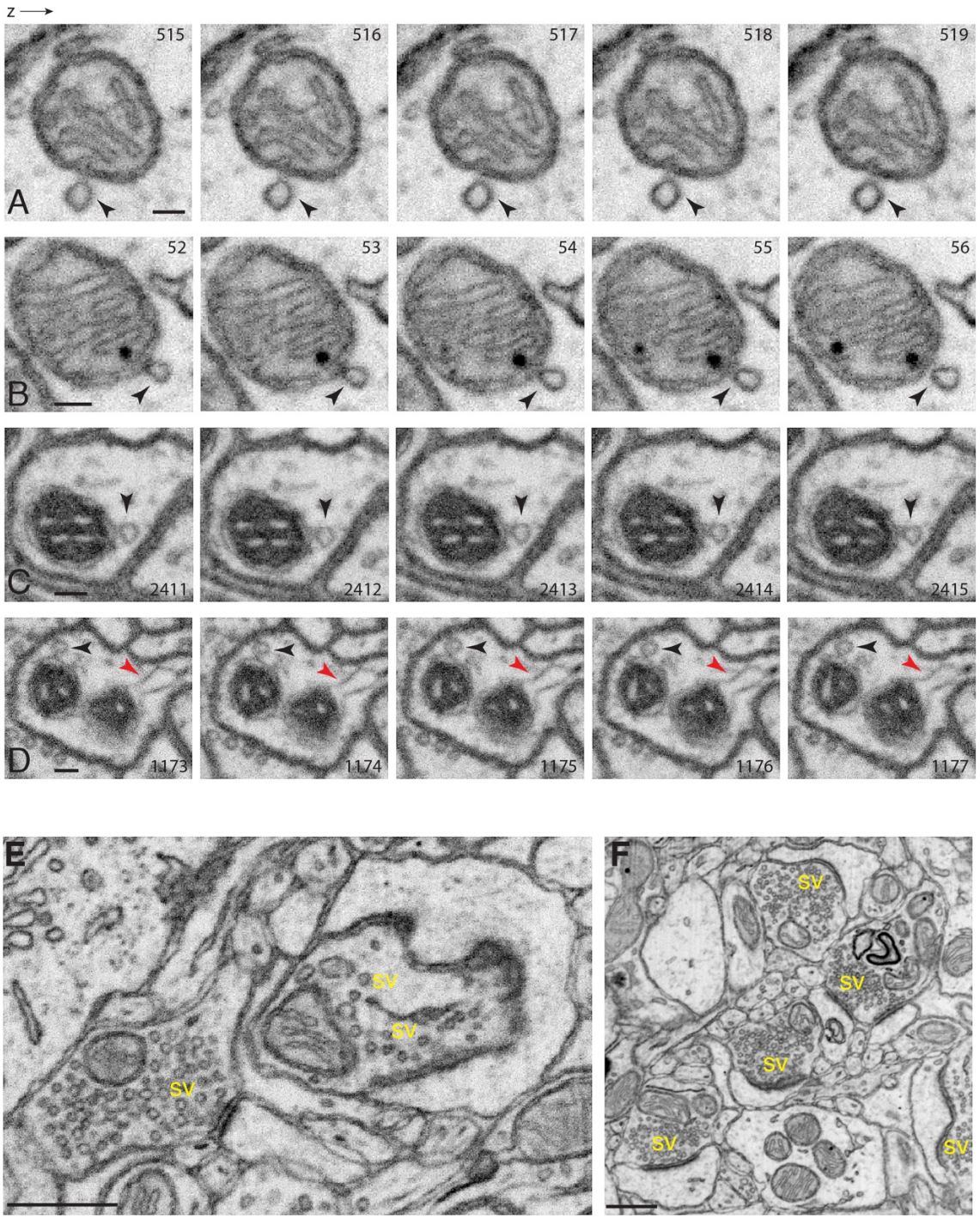

Figure S2. Definition of mitochondrial protrusions, and synapses, Related to Figure 3-5. (A-D) Examples of vesicles (black arrowheads) next to, but not a part of, mitochondria. Unlike the typical mitochondria protrusion (i.e., red arrowheads in D), these next-to-mitochondria-vesicles are not included in the analysis of this study. (A,B) FIB-SEM of the mouse nucleus accumbens. (C,D) FIB-SEM of the *Drosophila* protocerebral bridge. The voxel of both FIB-SEM stacks is 4x4x4 nm. The number on the micrograph indicates its z-position in the SEM image stack. (E,F) Structural features of synapse: presynaptic terminal containing synaptic vesicles (sv), synaptic cleft, and postsynaptic density. Scale bars in A to D, 100 nm, in E,F, 500 nm.

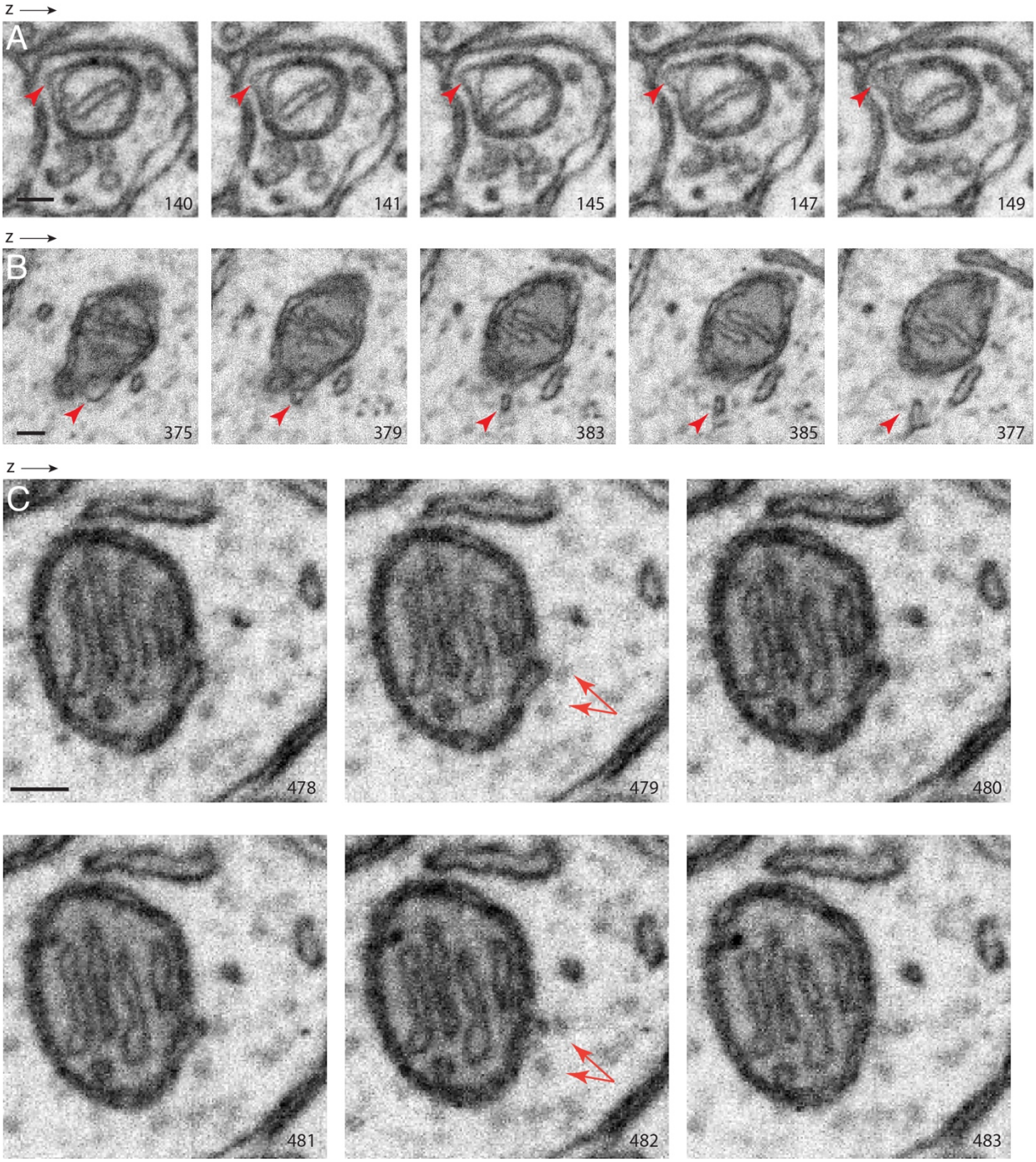

Figure S3. Additional examples of mitochondrial protrusions in neurons of the mouse nucleus accumbens revealed by FIB-SEM, Related to Figure 3. (A) A protrusion with a stubby neck. (B) An example of a small protrusion (arrowheads). (C) In this example, cross-section views of several microtubules are evident; red arrows indicate two of them; note the 1) light color compared to the membrane of adjacent tubulovesicular structures, 2) generally rounded shape in cross-section, and 3) occasional radial spokes. Also shown in this image series, a mitochondrial protrusion makes a direct contact with one of the microtubules (top arrow).The z-resolution of the SEM image stack is 4 nm. The number on the micrograph indicates its z-position in the image stack. Scale bar, 100 nm.

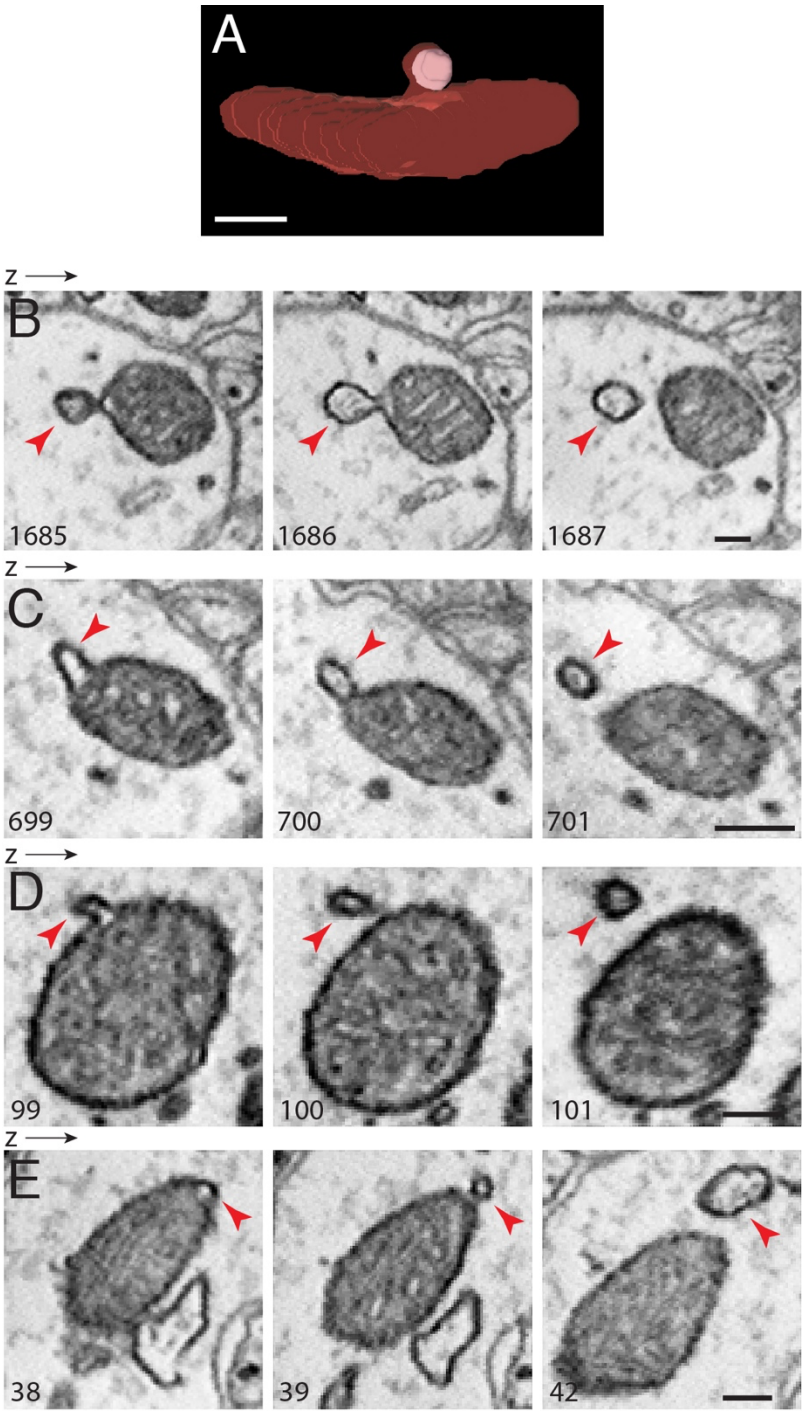

Figure S4. Additional examples of mitochondrial protrusions in neurons of the mouse cortex revealed by ATUM-SEM, Related to Figure 4. (A) A 3D reconstruction of a mitochondrion with a protrusion (see Figure 4A,a). (B-E) Examples showing mitochondrial protrusions in different shapes and sizes. The z-resolution of the EM image stack is 30 nm. The number on the micrograph indicates its z-position in the image stack. Scale bars, 100 nm.

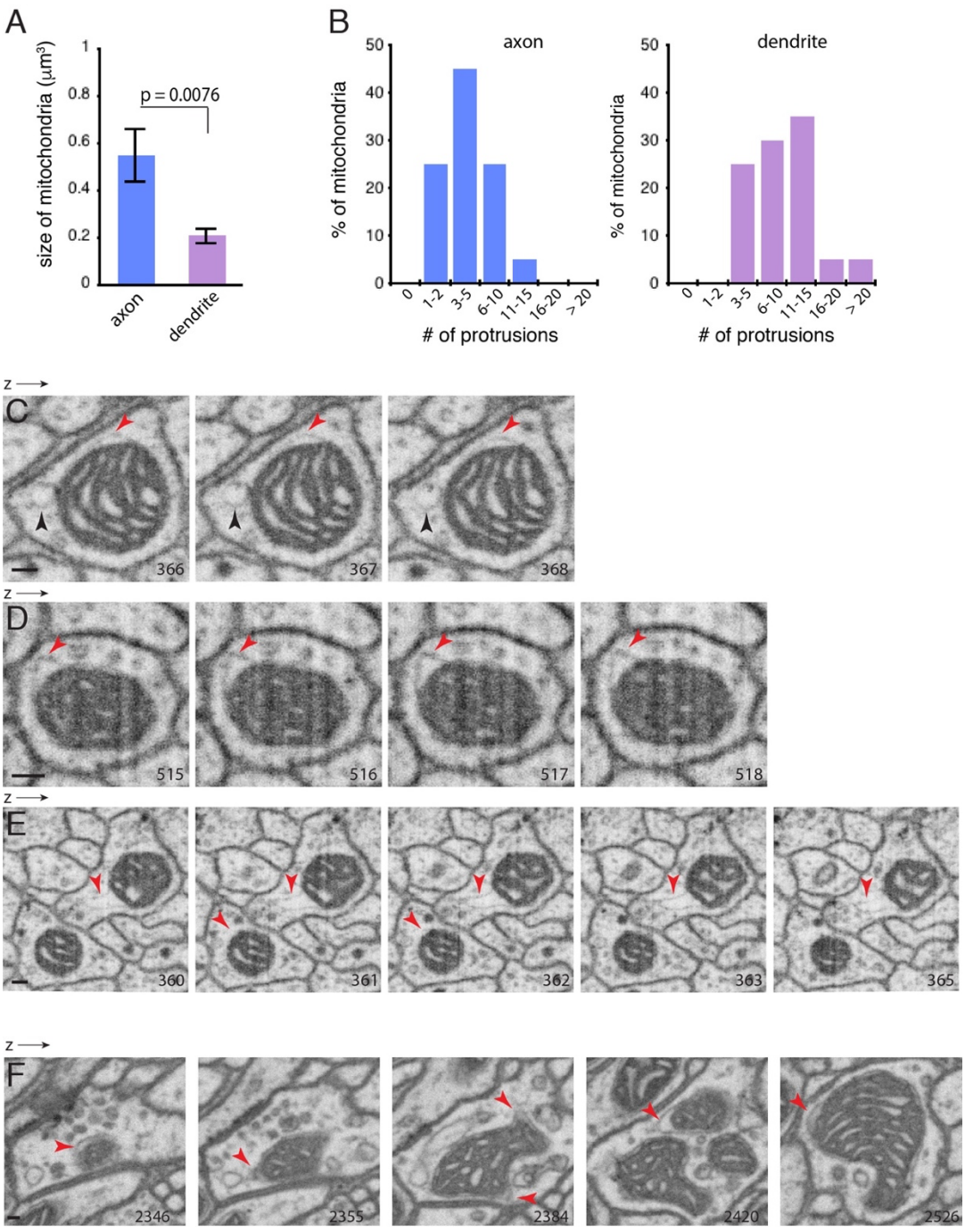

Figure S5. FIB-SEM examination of *Drosophila* neurons, Related to Figure 5. (A,B) Protocerebral bridge neurons. (A) Comparison of the size of axonal and dendritic mitochondria. Data are represented as mean ± SEM. Student's *t* test was used for calculating the p value. n = 20 axonal and 20 dendritic mitochondria. (B) Percentage of mitochondria with protrusions. (C-E) Mushroom body neurons. Examples show mitochondrial protrusions (red arrowheads) in different shapes and sizes. Black arrowheads indicate a vesicle next to but not a part of the mitochondrion. The voxel of the FIB-SEM is 4x4x4 nm. (F) A mitochondrion from a protocerebral bridge neuron shows multiple protrusions (red arrowheads). The number on the micrograph indicates its z-position in the SEM image stack. Scale bars, 100 nm.

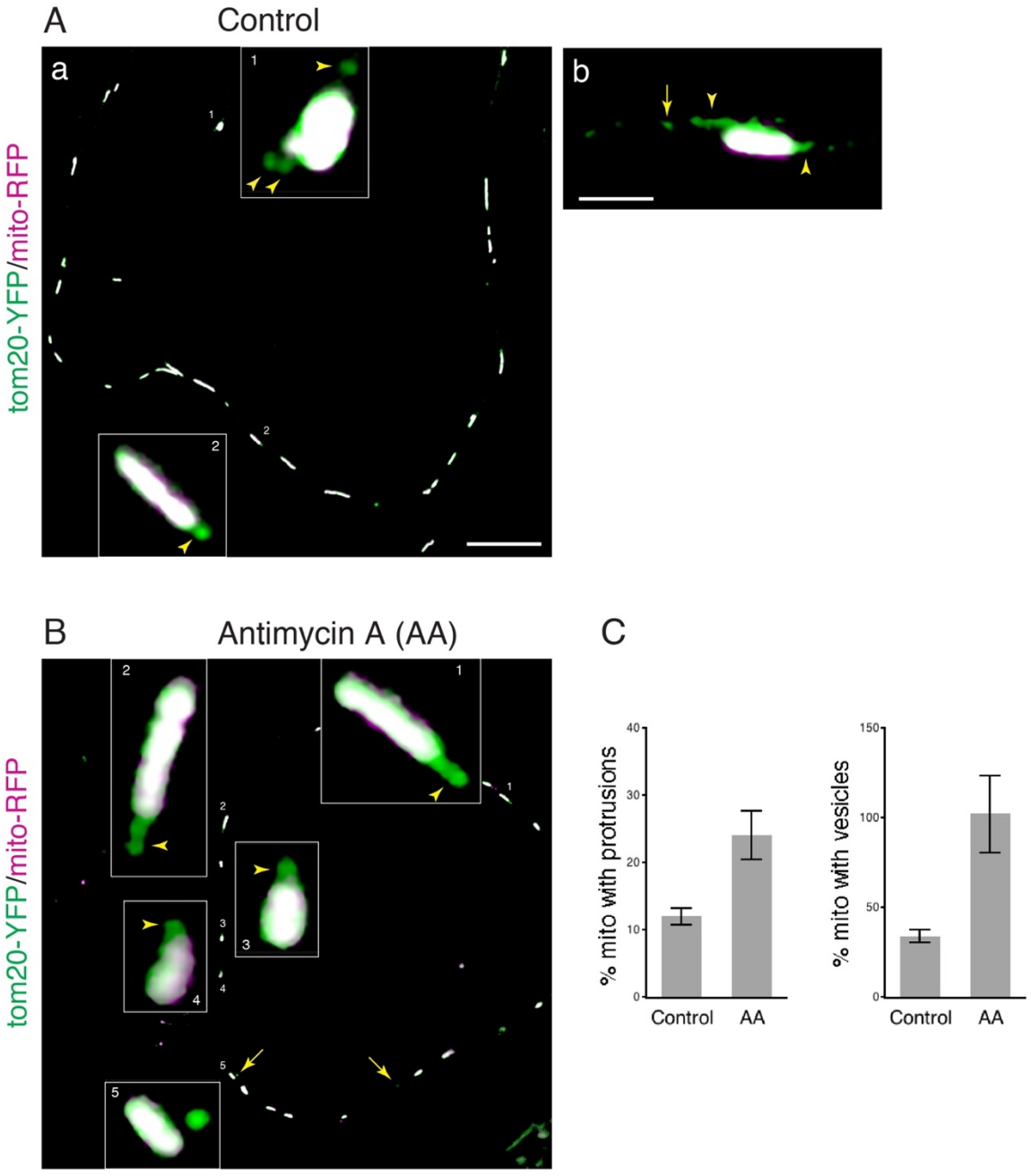

Figure S6. Fluorescence images of cultured hippocampal neurons expressing tom20-YFP and mito-RFP, Related to Figure 6. Boxed areas show enlarged views of tom20-YFP-illuminated mitochondrial protrusions (arrowheads) or vesicles (arrows). (A) untreated control; (B) AA-treated. (C) Percent of mitochondria with protrusions or vesicles (related to Figure 6H and Figure 6I, in which data are presented as number of mitochondrial protrusions or vesicles per mitochondrion). Data are represented as mean ± SEM. Student's *t* test was used for calculating the p values. $p < 0.01$ for analyses of both protrusions and vesicles. Scale bars in Aa and B, 10 mm; in Ab, 1 mm.

Transparent Methods

Animals

Adult male Sprague-Dawley rats were used for conventional transmission electron microscopy. Timed pregnant female Sprague-Dawley rats were used as the source of embryonic brain tissues for establishing cultures of hippocampal neurons. Planaria (*Dugesia tigrina*) were obtained from Carolina Biological Supplies. All animal procedures were approved by the NIA and NIDCD Animal Care and Use Committees and complied with the NIH Guide for Care and Use of Laboratory Animals. Animals used for producing the 3D EM datasets were described in the respective studies published previously (see below).

Reagents

DNA construct tom20-YFP was kindly provided by Dr. Chad Williamson (NICHD, NIH) and mito-RFP was kindly provided by Dr. Carolyn Ott (HHMI at Janelia Research Campus). Culture media and reagents including Neurobasal medium and B27 were from Invitrogen. Calcium phosphate mammalian transfection kit was from Clontech (#631312). Antimycin A (#A8674) and poly-L-lysine (#P2636) were from Sigma.

Transmission electron microscopy (TEM)

Sections of the rat hippocampi were prepared exactly as described in several of our previous studies (Petralia and Wenthold, 1999; Petralia et al., 1999; Petralia et al., 2010; Petralia et al., 2018). Briefly, rats were anesthetized and immediately transcardially perfused with 4% paraformaldehyde plus 0.5% glutaraldehyde. The brains were removed and post-fixed in the same fixative solution for 2 hours, and were vibratomed at 350 μm. The hippocampi were dissected from the brain sections, and were cryoprotected, frozen in a Leica EM CPC, and then embedded in Lowicryl in a Leica AFS freeze-substitution instrument. After staining with uranyl acetate and lead citrate, thin sections (from 3 rats) were examined in a JEOL JEM-2100 TEM microscope.

The planarian brains were prepared with the same procedure described above and used in previous studies (Petralia et al., 2015; Petralia et al., 2016). For the present study, new thin sections from the brains of 2 planaria were stained with uranyl acetate and lead citrate and examined in a JEOL JEM-2100 TEM microscope.

In both the rat hippocampus and planaria brains, definitive axons were identified by the presence of clusters of synaptic vesicles and/or a synapse; dendrites were identified by the presence of a synapse or characteristics of large dendrites, including a combination of tapering, even shape, microtubules, and multiple mitochondria and other organelles, as described (Petralia et al., 2010, Petralia et al., 2018). In the hippocampus, thin processes with the structural appearance of axons or thin dendrites, but without visible synapses, were defined as neurites. Also, in the hippocampus, large and irregular shaped processes with loose bundles of intermediate (i.e., glial filaments) were identified as glia processes.

FIB-SEM and ATUM-SEM datasets and analysis

The nucleus accumbens FIB-SEM dataset was produced in previous studies (Wu et al., 2017; Xu et al., 2017). The nucleus accumbens tissue was from an adult mouse (C57/BL6J). The mouse was transcardially perfused with a mixture of 2% glutaraldehyde and 2% depolymerized paraformaldehyde in 0.1 M phosphate buffer. The brain was removed and post-fixed in the same mixture overnight at 4^0C, and 50-μm sections were prepared. Following additional processing as detailed in Wu et al. (2017) and Xu et al. (2017), FIB-SEM of the nucleus accumbens was produced. The FIB-SEM dataset used in the present study has 562 serial EM images with a voxel of 4x4x4 nm.

The somatosensory cortex ATUM-SEM (automatic tape-collecting ultramicrotome-scanning electron microscopy) dataset was produced in a previous study (Kasthuri et al., 2015). The somatosensory cortex tissue (layer V or V/VI) was from an adult mouse (BALB/c). The mouse was transcardially perfused with 200 ml (~ 5 ml/min flow rate) of fixative solution containing 2% glutaraldehyde, 4% paraformaldehyde and 0.2 mM $CaCl_2$ in cacodylate buffer (0.1M, pH 7.4). The brain was removed and post-fixed in the same fixative solution overnight at 4^0C. The somatosensory cortex was then dissected, sectioned, and processed as described in detail in Kasthuri et al. (2015). The ATUM-SEM dataset of the somatosensory cortex consisted of 1850 serial EM images with a voxel of 6x6x30 nm.

The *Drosophilia* FIB-SEM of protocerebral bridge was produced as described previously (Takemura et al., 2017; Xu et al., 2017). Brain tissue was from a 5-day-old adult female CantonS G1xw1118 Drosophila. Vibratome brain slices (200 μm) were fixed in 2.5% glutaraldehyde and 2.5% paraformaldehyde in 0.1 M cacodylate for 10-15 min before processing for freeze-substitution, followed by embedding in Durcupan resin. Smaller vertical posts were then trimmed to the region of interest – protocerebral bridge – guided by X-ray tomography data obtained by a Zeiss Versa XRM-510 and optical inspection under a microtome. Details of the FIB-SEM production were described in detail previously (Xu et al., 2017).

We used VAST (Volume Annotation and Segmentation Tool)(Berger et al., 2018; Kasthuri et al., 2015) to visualize and annotate mitochondria in the brain SEM datasets. We examined mitochondria in axons and dendrites of neurons. Axonal mitochondria were identified as mitochondria in the synaptic vesicle-containing presynaptic terminals or in structures that can be traced to presynaptic terminals. Dendritic mitochondria were defined as mitochondria either in postsynaptic structures that directly form synaptic contact with presynaptic terminals, or in a dendrite, a part of which can be traced to form a synapse. Synapses of mouse neurons were identified based on the presence of synaptic vesicles, a synaptic cleft, and a clearly visible postsynaptic density (Figure S2E,F). Synapses of *Drosophila* protocerebral bridge neurons were identified based on the presence of synaptic vesicles, presynaptic T-bar, and postsynaptic density (i.e., Figure 5).

For assessing the number of mitochondria protrusions, we randomly selected mitochondria from axons or dendrites, and examined the mitochondria in their entirety in z-dimensions. For the mouse nucleus accumbens FIB-SEM dataset, a total of 58

axonal mitochondria and 42 dendritic mitochondria were examined. For the mouse somatosensory cortex ATUM-SEM dataset, 400 axonal mitochondria and 200 dendritic mitochondria were examined. For the *Drosophilia* FIB-SEM of protocerebral bridge dataset, 20 axonal mitochondria and 20 dendritic mitochondria were examined. For measuring the size of mitochondria in the *Drosophilia* protocerebral bridge neurons, we segmented the mitochondria in their entirety using VAST, then calculated the volume of the segmented mitochondria using MatLab (Berger et al., 2018). For 3D reconstruction of mitochondria, we used VAST followed by 3ds Max (Autodesk).

Neuron culture and transfection

Cultures of hippocampal neurons were prepared from embryonic day 18 rat brains using a described protocol (Kaech and Banker, 2006; Yao et al., 2015; Yao et al., 2017). Dissociated neurons were seeded at a density of ~200 cells/mm^2 on poly-L-lysine (1 mg/ml)-coated glass coverslips (no. 1.5) and grown in Neurobasal medium supplemented with B27. After growing in culture for 6 to 7 days (days in vitro), the neurons were transfected with tom20-YFP and mito-RFP using a calcium phosphate-based kit following the manufacturer's protocol (Clontech, #631312). Twenty-four hours after transfection, the neurons were incubated with 5 nM Antimycin A for 5 hours, followed by recovery in medium without Antimycin A for 1 hour. The neurons were immediately fixed in pre-warmed 4% paraformaldehyde and 4% sucrose for 15 minutes, and then washed gently, mounted in Prolong Gold antifade reagent, and stored at 4^{0}C before imaging. The experiments were repeated 5 times in 5 different batches of hippocampal neuronal cultures.

Fluorescence microscopy and analysis

Neurons expressing tom20-YFP and mito-RFP were examined, and images were acquired with an Apochromat 63x/1.4 numerical aperture objective lens on a Zeiss LSM 880 microscope with Airyscan (Carl Zeiss). All images were acquired at a 1024 x 1024-pixel resolution (1 pixel = 43.5 μm). In the present study, we focused on examining mitochondria in neurites in both control and experimental group. For each experiment, 10 images (67.8 μm^2 per image) from 2 coverslips were acquired. The image acquisition settings were kept the same between different experiments. The brightness, contrast, and levels of the images were adjusted evenly across the image for each channel in Adobe Photoshop and compiled in Adobe Illustrator. No additional digital image processing was performed.

Mitochondrial protrusions were visualized in Photoshop (after using the Auto Tone once) and defined with the following criteria: (1) protruding from - but still connecting to - mitochondria; (2) tom20-YFP positive; (3) mito-RFP negative - confirmed by the absence of RFP signal in individual RGB channels. The number of these mitochondrial protrusions were counted manually. Mitochondrial vesicles were defined as tom20-YFP positive puncta that were not connected to mitochondria. The number of these mitochondrial vesicles were counted using the Analyze Particles in imageJ with the particle size set at 5-100 pixel units. The number of mitochondria, which co-

express tom20-YFP and mito-RFP, were also counted using the Analyze Particles in image J with the particle size set at 100-infinity pixel units.

Statistical Analysis

Statistical analysis was performed using KaleidaGraph and Graphpad Prism. For comparison of two groups (Figure 6H-K; Figure S5A; Figure S6C), statistical significance was determined by two-tailed Student's *t* test. To determine the correlation (Figure 5I), Pearson's correlation analysis was used. Data are represented as mean ± SEM. The number of experimental replicates can be found in the figure legends. A p-value of < 0.05 was considered as a threshold for statistical significance. All p values are listed on the figures.

Transparent Methods References

Berger, D.R., Seung, H.S. and Lichtman, J.W. (2018). VAST (Volume Annotation and Segmentation Tool): Efficient Manual and Semi-Automatic Labeling of Large 3D Image Stacks. Front Neural Circuits. 12, 88

Kaech, S. and Banker, G. (2006). Culturing hippocampal neurons. Nat Protoc. 1, 2406-2415.

Kasthuri, N., Hayworth, K.J., Berger, D.R., Schalek, R.L., Conchello, J.A., Knowles-Barley, S., Lee, D., Vázquez-Reina, A., Kaynig, V., Jones, T.R., Roberts, M., Morgan, J.L., Tapia, J.C., Seung, H.S,. Roncal, W.G., Vogelstein, J.T., Burns, R., Sussman, D.L., Priebe, C.E., Pfister, H. and Lichtman, J.W. (2015). Saturated Reconstruction of a Volume of Neocortex. Cell. 162, 648-661.

Petralia, R.S. and Wenthold, R.J. (1999). Immunocytochemistry of NMDA receptors.Methods Mol Biol. 128, 73-92.

Petralia, R.S., Esteban, J..A, Wang, Y.X., Partridge, J.G., Zhao, H.M., Wenthold, R.J. and Malinow, R. (1999). Selective acquisition of AMPA receptors at hippocampus CA1 synapses during postnatal development. Nature Neurosci. 2, 31-36.

Petralia, R.S., Wang, Y.X., Hua, F., Yi, Z., Zhou, A., Ge, L., Stephenson, F.A. and Wenthold, R.J. (2010). Organization of NMDA receptors at extrasynaptic locations. Neuroscience. 167, 68-87.

Petralia, R.S., Wang, Y.X., Mattson, M.P. and Yao PJ. (2018). Invaginating Structures in Mammalian Synapses. Front Synaptic Neurosci. 10, 4.

Petralia, R.S., Wang, Y.X., Mattson, M.P. and Yao, P.J. (2015). Structure, Distribution, and Function of Neuronal/Synaptic Spinules and Related Invaginating Projections.

Neuromolecular Med. 17, 211-240.

Petralia, R.S., Wang, Y.X., Mattson, M.P. and Yao ,P.J. (2016). The Diversity of Spine Synapses in Animals. Neuromolecular Med. 18, 497-539.

Wu, Y., Whiteus, C., Xu, C.S., Hayworth ,K.J., Weinberg, R.J., Hess, H.F. and De Camilli, P. (2017). Contacts between the endoplasmic reticulum and other membranes in neurons. Proc Natl Acad Sci. 114, E4859-E4867.

Xu, C.S., Hayworth, K.J., Lu, Z., Grob, P., Hassan, A.M., García-Cerdán, J.G., Niyogi, K.K., Nogales, E., Weinberg, R.J. and Hess, H.F. (2017). Enhanced FIB-SEM systems for large-volume 3D imaging. Elife. 6, e25916.

Yao, P.J., Manor, U., Petralia, R.S., Brose, R.D., Wu, R.T., Ott, C., Wangm Y.X., Charnoff, A., Lippincott-Schwartz, J. and Mattson, M.P. (2017). Sonic hedgehog pathway activation increases mitochondrial abundance and activity in hippocampal neurons. Mol Biol Cell 28, 387-395

Yao, P.J., Petralia, R.S., Ott, C., Wang, Y.X., Lippincott-Schwartz, J. and Mattson, M.P. (2015). Dendrosomatic Sonic Hedgehog Signaling in Hippocampal Neurons Regulates Axon Elongation. J Neurosci. 35, 16126-16141